

PROCEEDINGS OF SPIE

SPIDigitalLibrary.org/conference-proceedings-of-spie

Non-rigid registration to determine strain fields during mouse brain fixation and embedding

Rodgers, Griffin, Schulz, Georg, Kuo, Willy, Scheel, Mario, Kurtcuoglu, Vartan, et al.

Griffin Rodgers, Georg Schulz, Willy Kuo, Mario Scheel, Vartan Kurtcuoglu, Timm Weitkamp, Bert Müller, Christine Tanner, "Non-rigid registration to determine strain fields during mouse brain fixation and embedding," Proc. SPIE 11586, Bioinspiration, Biomimetics, and Bioreplication XI, 115860I (31 March 2021); doi: 10.1117/12.2583632

SPIE.

Event: SPIE Smart Structures + Nondestructive Evaluation, 2021, Online Only

Non-rigid registration to determine strain fields during mouse brain fixation and embedding

Griffin Rodgers^{a,b}, Georg Schulz^{a,b,c}, Willy Kuo^{d,e}, Mario Scheelf, Vartan Kurtcuoglu^{d,e}, Timm Weitkamp^f, Bert Müller^{a,b}, and Christine Tanner^{a,b}

^aBiomaterials Science Center, Department of Biomedical Engineering, University of Basel, 4123 Allschwil, Switzerland

^bBiomaterials Science Center, Department of Clinical Research, University Hospital Basel, 4031 Basel, Switzerland

^cCore Facility Micro- and Nanotomography, Department of Biomedical Engineering, University of Basel, 14, 4123 Allschwil, Switzerland

^dThe Interface Group, Institute of Physiology, University of Zurich, 8057 Zurich, Switzerland

^eNational Centre of Competence in Research, Kidney.CH, 8057 Zurich, Switzerland

^fSynchrotron Soleil, 91192 Gif-sur-Yvette, France

ABSTRACT

Biological matter may change shape *via* water absorption or loss. For example, brain tissue shows non-uniform shrinkage during formalin fixation and paraffin embedding, which is the most common tissue preparation for conventional histological analysis. Local deformations can be analyzed with non-rigid registration of non-destructive three-dimensional imaging datasets. We utilized synchrotron radiation microtomography at the ANATOMIX beamline of Synchrotron SOLEIL to image a mouse brain with 3 micron voxel length after formalin fixation, immersion in ascending alcohol series and xylene, and after paraffin embedding. We created a pipeline for non-rigid registration to align the volumes and extract volumetric strain fields. In this way, we could visualize the swelling/shrinkage of anatomical features. This method avoids time-consuming segmentation of brain regions, however it is sensitive to the registration parameters. In this proceedings paper, we discuss the selection of registration parameters in order to generate plausible volumetric strain fields. This protocol can be deployed to any type of shape change of biological matter and allows for the quantification of the related processes.

Keywords: mouse brain, hard X-ray computed tomography, microtomography, synchrotron radiation, image registration, strain field, embedding-induced local deformation

1. INTRODUCTION

Biological matter may change shape *via* water absorption or loss. A prominent example is the pine cone.¹ In humid weather, pine cones fold their scales to prevent seeds from spreading. On a dry day, the scales gape open to release the seeds. Another fascinating example is the water-induced color change of male *Hoplia coerulea* beetles, whose color can change from green to blue during the day.²

In the context of high resolution neuroimaging, shape change is observed as an unwanted byproduct of fixation, water loss, and solvent exchange during tissue preparation.^{3,4} First, fixation of *post mortem* tissue with e.g. formalin induces unavoidable morphological changes.⁵ Further deformations are induced by additional preparation steps common for histological analysis,⁶ namely immersion in ethanol, xylene, and embedding into a solid paraffin block (see Figure 1). Therefore, evaluating the accuracy of post mortem neuroimaging data with respect to the *in vivo* situation is challenging.

The goal of this study was to combine three-dimensional imaging with non-rigid registration to quantify and correct morphological changes in a mouse brain from the formalin fixed state *via* immersion in ascending ethanol

Further author information: (Send correspondence to G.R.) E-mail: griffin.rodgers@unibas.ch, Telephone: +41 61 207 54 38, www.bmc.unibas.ch

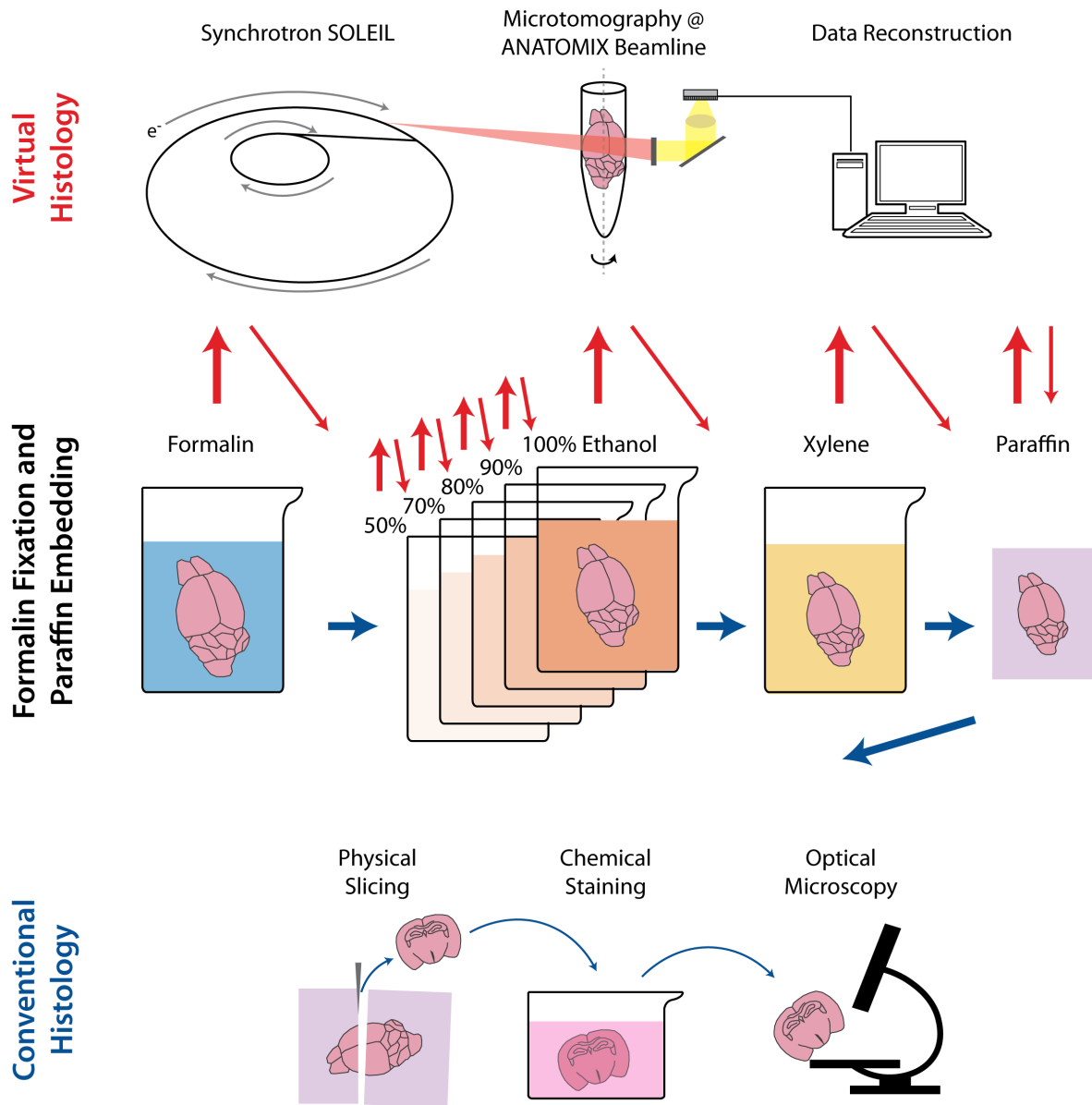


Figure 1. Experiment design. Formalin fixation and embedding is the standard procedure in conventional histology and is combined with subsequent slicing, staining, and optical microscopy (blue arrows). Virtual histology based on non-destructive X-ray imaging is complementary to conventional histology and can be applied at any preparation step. Here, synchrotron-radiation based microtomography was utilized to measure an entire mouse brain after two hours of immersion in each embedding medium (red arrows). Imaging of the full mouse brain with $3.1\ \mu\text{m}$ voxel length was performed at the ANATOMIX beamline, Synchrotron SOLEIL (Gif-sur-Yvette, France).

solutions and xylene to embedding in a paraffin block. Therefore, we utilized synchrotron radiation-based X-ray micro computed tomography to image the entire mouse brain with $3.1\ \mu\text{m}$ voxel length (Figure 1). The choice of registration parameters, in particular the regularization, had a strong effect on the calculated volumetric strain fields. As the ground truth deformations are unknown, validation of the non-rigid registration is challenging.⁷⁻⁹ In this proceedings paper, we discuss a method for the selection of registration parameters in order to generate plausible volumetric strain fields.

2. MATERIALS AND METHODS

2.1 Mouse brain fixation and embedding

The brain used in this experiment was excess material from an experiment with approval of the veterinary office of the Canton of Zurich (license number ZH067/17). After death, the brain was extracted from a seven-month-old male C57BL/6J mouse (Janvier Labs, Le Genest-Saint-Isle, France) and fixed by immersion in 4% formaldehyde solution (Sigma Aldrich, Darmstadt, Germany) and subsequently immersed in 50%, 70%, 80%, 90%, and 100% ethanol solutions and xylene for two hours each (Carl Roth GmbH, Karlsruhe, Germany). Between each step, the entire brain and some surrounding solution was placed in a 1.5 mL Eppendorf tube for microtomography measurements. Finally, the brain was transferred to liquid paraffin wax (ROTI[®] Plast, Carl Roth GmbH, Karlsruhe, Germany) at a temperature of 60°C for 2 hours then cooled to create a solid paraffin block. This block was trimmed to remove excess paraffin before measurement.

2.2 Synchrotron radiation-based virtual histology

Hard X-ray microtomography was performed at the ANATOMIX Beamline (Synchrotron SOLEIL, Gif-sur-Yvette, France).¹⁰ An undulator gap of 10.3 mm and a 20 μm Au filter created a polychromatic beam with mean energy around 22 keV. Images were recorded on a detector consisting of a 300 μm LuAG scintillator coupled to a scientific CMOS camera (Hamamatsu Orca Flash 4.0 V2, 2048 \times 2048 pixels, 6.5 μm physical pixel size) by two photo objectives in tandem geometry (Hasselblad HC 4/210 and HC 2.2/100, 0.22 numerical aperture).¹¹ The resulting magnification factor was 2.1, yielding an effective pixel size of 3.1 μm . Spatial resolution was measured to be just below 10 μm based on radiographs of a Siemens star test pattern.

For tomographic imaging, 5,900 projections were acquired around 360° with the rotation axis off-center to double the detector field-of-view. The scans were done “on the fly” with continuous rotation to reduce overhead. The exposure time was 50 ms and a single scan took seven minutes. The field-of-view was extended vertically to image the entire brain by stitching together three to four height steps.

Tomographic reconstruction was done in `Matlab` (The MathWorks, Inc., Natick, USA) using the filtered back-projection algorithm with the standard Ram-Lak filter. To reduce noise at the expense of spatial resolution, a Gaussian filter with $\sigma = 1.25$ pixels was applied to the unbinned data.¹² Additional reconstructions were made with 3 \times and 9 \times binning to reduce noise and data size.¹³

2.3 Non-rigid registration

Non-rigid registration was based on `elastix`,^{14,15} an open-source software toolbox. The non-rigid registration pipeline consisted of three steps: (1) coarse manual affine pre-alignment, (2) automatic multi-resolution affine

Table 1. Parameters for registration steps 1, 2, and 3: manual pre-alignment, automatic affine, and automatic non-rigid registration. The registration pipeline was designed for texture-enhanced 3 \times 3 \times 3 binned datasets, each approximately 1,305 \times 1,305 \times 2,144 voxels in size (\approx 7 GB in size at 16-bit depth). The approximate time for each step is given for a workstation with a Intel[®] Xeon[®] 16 core CPU (E5-2637 v2, 3.50GHz) and 144 GB memory.

	Step 1	Step 2	Step 3
manual/automatic	manual	automatic	automatic
transformation model	similarity	affine	B-spline
degrees of freedom	7	12	\approx 7 million
optimizer	-	Adaptive Stochastic Gradient Descent	Adaptive Stochastic Gradient Descent
# spatial samples	-	65,536	131,072
# iterations	-	1,000	2,000
# resolutions	-	4	5
similarity metric	-	Mattes mutual information	Mattes mutual information
approx. time	1.5 minutes	30 minutes	450 minutes

registration, and (3) automatic multi-resolution B-spline registration. A final rigid transformation (4) was used for displaying the data in anatomical planes. The open-source program `transformix`^{14,15} was used to calculate volumetric strain fields from the determinant of the spatial Jacobian of the composition of transformations (1)-(4).

Section 3.1 discusses the selection of the basic parameters. Section 3.2 presents the criteria for selection of the regularization term for step (3). Section 3.3 presents the resulting registration and volumetric strain fields. Details of the registration pipeline are given in Table 1. The registration pipeline was designed for $3 \times 3 \times 3$ binned datasets, each approximately $1,305 \times 1,305 \times 2,144$ voxels in size (≈ 7 GB in size at 16-bit depth). A workstation with an Intel[®] Xeon[®] 16 core CPU (E5-2637 v2, 3.50 GHz) and 144 GB memory was used for the registrations.

3. RESULTS AND DISCUSSION

3.1 Selection of basic registration parameters

The formalin dataset was selected as the reference volume for all registrations as it was the closest to the physiological state. Preliminary registration of the $9 \times$ binned datasets showed that a manual pre-alignment step was necessary. Therefore, a rough alignment of all datasets (three translations, three rotations, and a scaling factor) was performed in the open-source three-dimensional visualization software `ITKSNAP`.¹⁶ These parameters were given as an initial transformation for the subsequent automatic registration steps.

Initial tests based on the $9 \times$ binned datasets also showed that the sample holder and surrounding medium presented strong features that affected registration. A semi-automatic segmentation of the brain generated binary masks for exclusion of these features from the registration optimization.

At 16-bit depth, the unbinned datasets were all over 100 GB in size. The standard workflow for `elastix` and `transformix` involves storing the entire reference and moving volumes in addition to other parameters such as masks and B-spline control point positions in memory. Therefore, the $3 \times$ binned datasets were selected for registration as the unbinned volumes could not be processed with our workstation with 144 GB of memory. The downsampled data offered the benefit of reduced noise.¹³

Affine registration was performed with both Mattes mutual information and normalized cross correlation as similarity metrics. In addition, both the standard volumes and texture enhanced volumes with standard deviation filtering of a $3 \times 3 \times 3$ voxel neighborhood were tested. Based on visual inspection of these registrations, Mattes mutual information and texture enhancement were chosen. The same tests for the non-rigid registration were inconclusive, therefore Mattes mutual information and texture enhancement were used for non-rigid registration to maintain consistency with the affine registration step.

For optimization, adaptive stochastic gradient descent was selected, as it is faster and more robust than the standard gradient descent.¹⁷ A multi-resolution approach was used to improve registration quality and avoid local minima traps.¹⁸ The affine step used 4 resolutions and the non-rigid step used 5 resolutions, both relying on smoothing and downsampling. Thanks to the downsampling, these lower resolution steps did not add significantly to the registration time.

By analyzing the image similarity as a function of the iteration number (examples of these curves can be seen in Figure 2), the number of spatial samples and iterations could be selected. A larger number of iterations led to a less noisy optimization curve and greater final image similarity at the expense of time. The number of iterations is linearly related to the registration time and could be chosen to ensure that the optimization curves were saturated. The final image similarity typically showed a plateau at a certain number of spatial samples, and the parameter was set to around that value.

Table 1 summarizes the parameters used for registration steps (1)-(3).

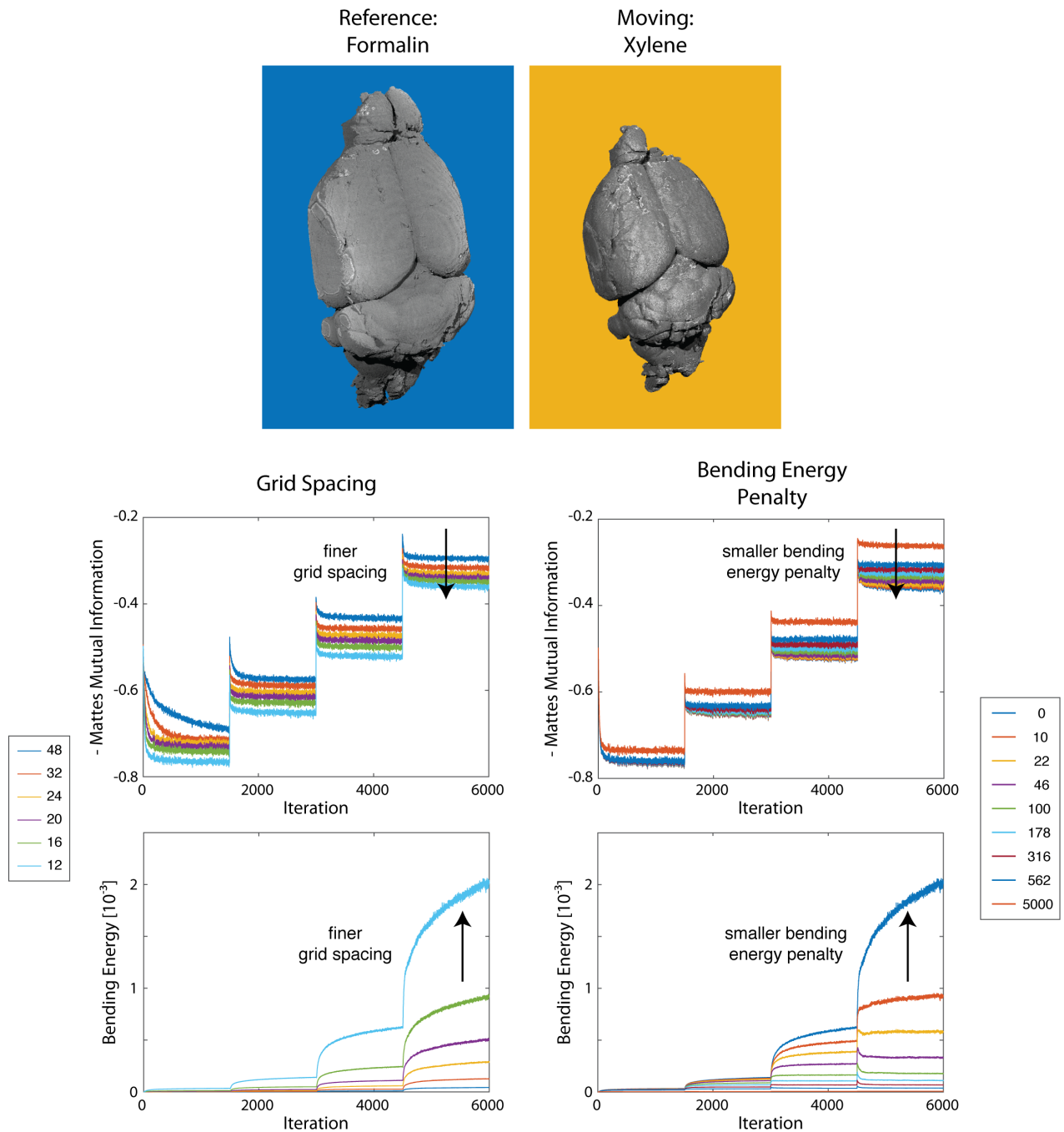


Figure 2. Selection of registration parameters. A series of registrations were run with formalin as reference and xylene as the moving image (top, volume renderings) in order to determine the registration parameters. Here, four resolutions with 1,500 iterations each were chosen to speed up the test registrations. A series of B-spline grid spacings [voxels] (left, with zero bending energy penalty) and bending energy penalties (right, with 12 voxel B-spline grid spacing) were tested to investigate the effect of regularization. The image similarity metric, here Mattes mutual information (top row), and bending energy (bottom row) were tracked. Decreasing regularization (finer grid spacing or smaller bending energy penalty) led to higher image similarity but also sharper local changes in the deformation field as measured by bending energy.

3.2 Regularization of the non-rigid registration

Visual inspection of the affine registration indicated that more degrees of freedom were needed to precisely align structures of the brain. A non-rigid registration based on B-splines was selected for this reason.¹⁹ The B-spline transformation is defined by a grid of control points, where each has an associated displacement vector. These displacement vectors are interpolated by cubic B-splines and thereby influence the displacement field within its neighbourhood of ± 2 grid spacings. The grid spacing of these control points therefore defines the degrees of freedom and controls the possible deformations: A finer grid spacing allows for sharply varying local deformations and a larger grid spacing only allows for smooth deformations.

Increasing the number of degrees of freedom typically brings greater image similarity, but gains are diminishing and come at the expense of potentially unrealistic deformations. In fact, visual inspection of sub-volume registrations with very small grid spacing (down to 4 voxels) showed no significant improvement or even poorer performance with the appearance of “wavy” edges. To counter this, regularization can be added by means of restricting the grid spacing or by adding a bending energy penalty to the cost function.

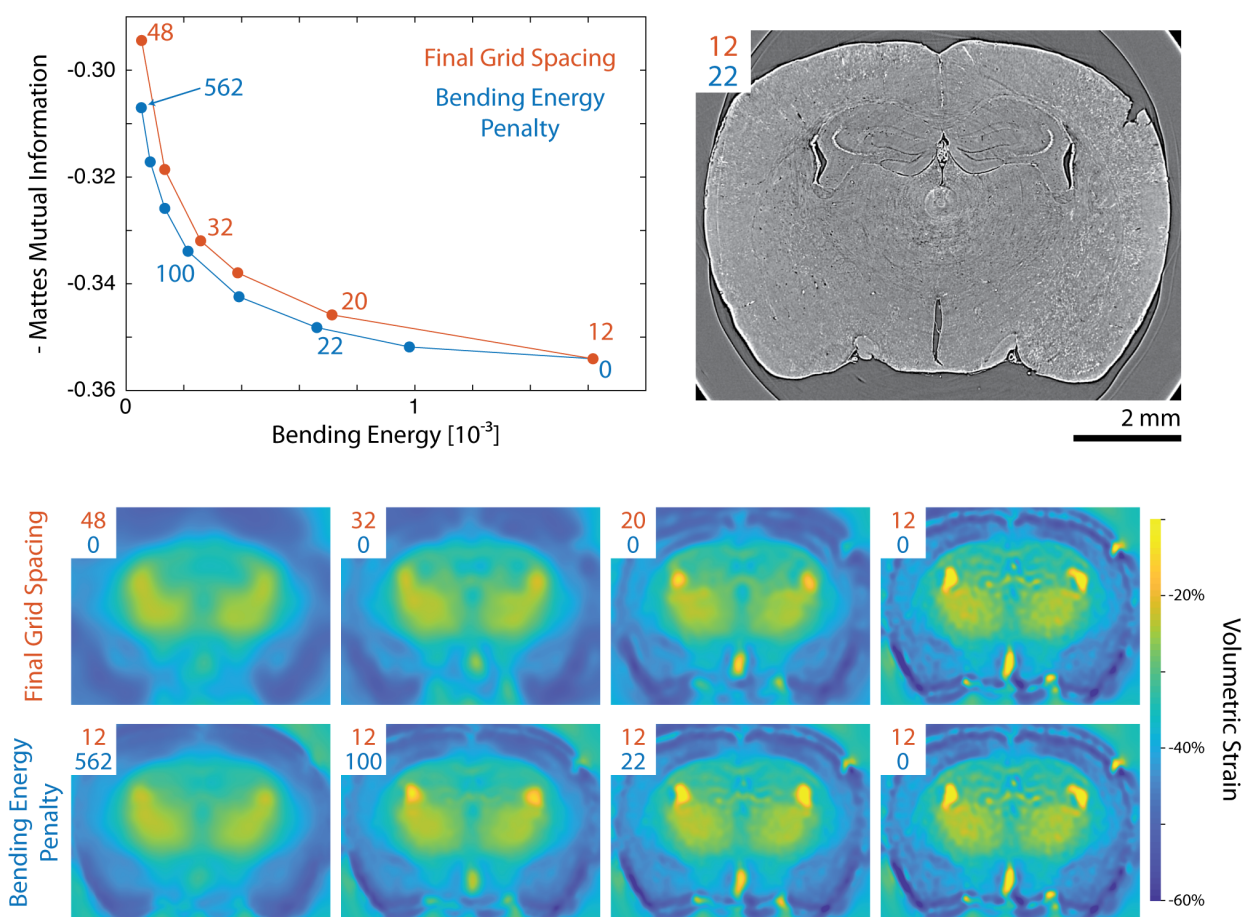


Figure 3. L-curve and Pareto fronts for registration regularization. The degree of regularization controls the trade-off between image dissimilarity and bending energy (orange: B-spline grid spacing [voxels]; blue: bending energy penalty). The curves have a characteristic L-shape. A fine grid spacing with bending energy penalty provides a more Pareto-efficient solution than increasing grid spacing without any bending energy penalty—as seen by the blue curve lying closer to $[0, -1]$. The related volumetric strain fields are shown for a region of interest containing the hippocampus and ventricles (upper right, gray scale corresponding to $\mu \pm 2\sigma$ of gray values in the volume). Unsurprisingly, increasing regularization (larger grid spacing or larger bending energy penalty) leads to more uniform volumetric strain fields, while decreasing regularization generates unrealistic strain variations in homogenous regions.

To determine the type and degree of regularization, two series of registrations were performed with the xylene-immersed brain as the moving volume (Figure 2): the first with no bending energy penalty and grid spacing from 48 to 12 voxels (this was the finest that could be run in the memory of our workstation), the second with the 12 voxel grid spacing and bending energy penalty ranging from 0 to 5,000. The image similarity and bending energy were tracked and were plotted as a function of the iteration in Figure 2. Unsurprisingly, the same trend was observed for both series: Increasing regularization led to lower bending energy and lower image similarity. In both cases, however, it appeared that increases in image similarity were diminishing for low regularization, while bending energy was greatly increasing.

Given the trade-off between bending energy and image similarity, no optimal solution can be found to simultaneously minimize bending energy and maximize image similarity. Therefore, we considered the Pareto efficiency of the two regularization approaches by plotting the final image similarity versus the final bending energy of each registration in the two series (Figure 4). These plots have the characteristic L-curve shape.²⁰ Regularization by means of a bending energy penalty was more Pareto efficient than by means of grid spacing. Therefore, we selected bending energy penalty as the method of regularization. We note that reduced grid spacing provides faster registrations, therefore it may still be a good choice for large datasets.

An additional consideration for the selection of the regularization parameter was that the resulting registration should generate plausible volumetric strain fields. As there is no ground truth and no metric to quantify this “plausibility”, we relied on a combination of visual inspection and the L-curve criterion.²⁰ Virtual slices through the volumetric strain fields are shown as a function of the regularization in Figure 3. With decreasing regularization, strain fields are less homogenous and considered unrealistic when variations occur within homogenous regions. On the other hand, the registration appears unrealistically over-regularized when clear borders of anatomical regions can not be distinguished (e.g. ventricles, isocortex, etc.). This visual inspection favored a level of regularization that corresponded to the bend in the L-curve, i.e. bending energy between 22 and 100. This agrees with the L-curve criterion, which amounts to selecting the corner of the L.²⁰

3.3 Final registration and volumetric strain fields

The regularization parameters for the final registrations were bending energy penalty of 30 and a grid spacing of 12 voxels. This grid spacing corresponded to ≈ 7 million degrees of freedom. The final registration and resulting volumetric strain fields are visualized for the xylene-immersed brain in Figure 4. The distribution of volumetric strain within the brain is also given.

The registration shows accurate alignment of most internal structures of the brain, e.g. within the hippocampus (Figure 4, color overlays). Even cellular resolution features such as the pyramidal layer of the hippocampus are precisely aligned. The poorest performance is observed in areas of extreme deformations, e.g. the third ventricle (right column).

The resulting volumetric strain fields show clear anatomical borders, but are relatively homogenous within anatomical regions. This is seen within the thalamus or isocortex in the coronal virtual slice through the volumetric strain field (Figure 4, upper right strain field).

4. CONCLUSION

Synchrotron radiation-based X-ray microtomography was used to visualize an entire mouse brain with 3.1 μm voxel length after each step of the conventional procedure for formalin fixation and paraffin embedding. In this report, we described the important considerations for building a pipeline for non-rigid registration of the datasets. We selected the type and degree of regularization based on Pareto efficiency, the L-curve criterion, and visual inspection of volumetric strain fields. The resulting registrations show accurate alignment of anatomical features down to the cellular level as well as plausible volumetric strain fields. This combination of three-dimensional imaging and non-rigid registration can be deployed to any type of shape change of biological matter and allows for the quantification of the related processes.

ACKNOWLEDGMENTS

The imaging was carried out under Synchrotron SOLEIL experiment No. 20190424. The authors thank J. Perrin and D. Guillaume of the ANATOMIX beamline at Synchrotron SOLEIL for support during the beam time. ANATOMIX is an Equipment of Excellence (EQUIPEX) funded by the Investments for the Future program of the French National Research Agency (ANR), project NanoimagesX, grant no. ANR-11-EQPX-0031. W.K. and V.K. acknowledge support from the Swiss National Science Foundation *via* NCCR Kidney.ch. G.R., C.T., and B.M. acknowledge support from the Swiss National Science Foundation Project No. 185058.

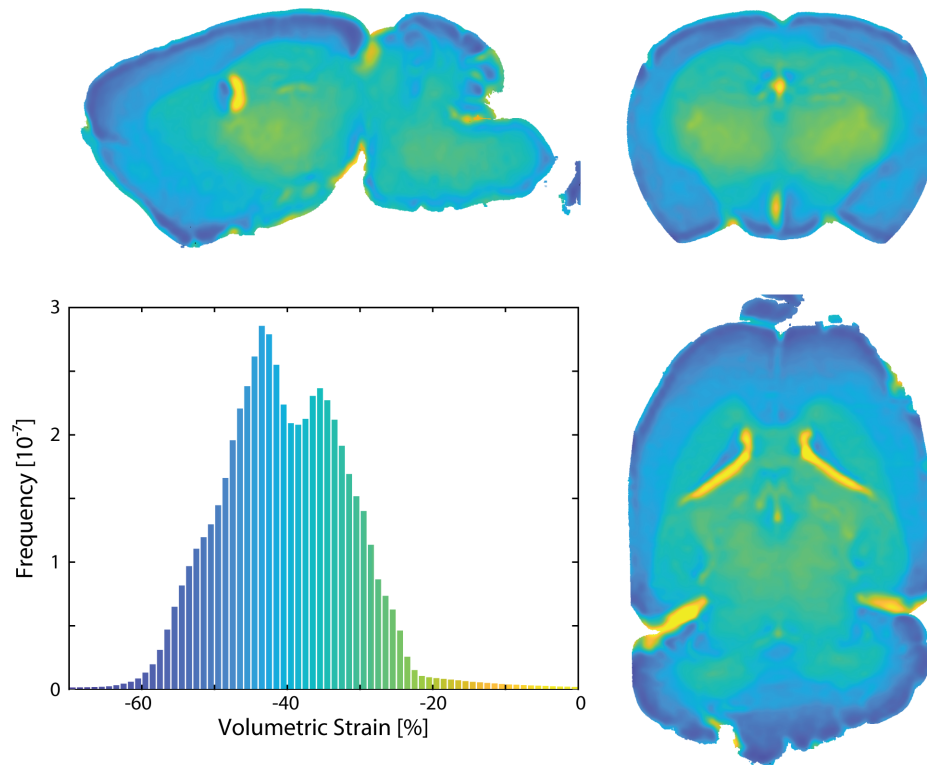
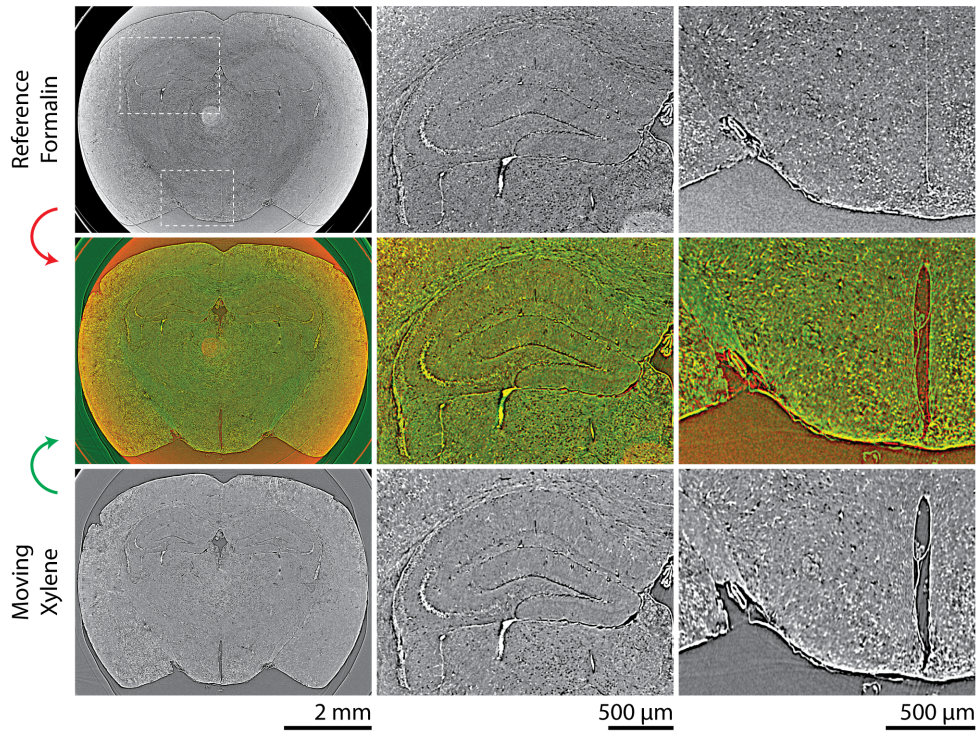


Figure 4. Registration results and volumetric strain field for the xylene immersed brain. The final registration used a grid spacing of 12 vx and bending energy penalty of 30. Results are visualized with a virtual coronal slice and zoom-ins (top). The volumetric strain fields are displayed for three orthogonal virtual slices (bottom). The result still shows clear borders between anatomical regions, but the regularization has reduced the variations within homogenous regions. The histogram of volumetric strain is also shown.

REFERENCES

- [1] Song, K., Yeom, E., Seo, S.-J., Kim, K., Kim, H., Lim, J.-H., and Joon Lee, S., “Journey of water in pine cones,” *Scientific Reports* **5**(1), 9963 (2015).
- [2] Rassart, M., Simonis, P., Bay, A., Deparis, O., and Vigneron, J. P., “Scale coloration change following water absorption in the beetle *hoplia coerulea* (coleoptera),” *Physical Review E* **80**, 031910 (2009).
- [3] Hardy, W. B., “On the structure of cell protoplasm,” *The Journal of Physiology* **24**(2), 158–210 (1899).
- [4] Quester, R. and Schröder, R., “The shrinkage of the human brain stem during formalin fixation and embedding in paraffin,” *Journal of Neuroscience Methods* **75**(1), 81 – 89 (1997).
- [5] Schulz, G., Crooijmans, H. J. A., Germann, M., Scheffler, K., Müller-Gerbl, M., and Müller, B., “Three-dimensional strain fields in human brain resulting from formalin fixation,” *Journal of Neuroscience Methods* **202**(1), 17 – 27 (2011).
- [6] Culling, C., “Chapter 2: Methods of examination of tissues and cells,” in [*Handbook of Histopathological and Histochemical Techniques*], Culling, C., ed., 19 – 25, Butterworth-Heinemann, 3rd ed. (1974).
- [7] Crum, W., Griffin, L., Hill, D., and Hawkes, D., “Zen and the art of medical image registration: correspondence, homology, and quality,” *NeuroImage* **20**(3), 1425–1437 (2003).
- [8] Schnabel, J. A., Tanner, C., Castellano-Smith, A. D., Degenhard, A., Leach, M. O., Hose, D. R., Hill, D. L., and Hawkes, D. J., “Validation of nonrigid image registration using finite-element methods: application to breast MR images,” *IEEE Transactions on Medical Imaging* **22**(2), 238–247 (2003).
- [9] Pluim, J. P., Muenzing, S. E., Eppenhof, K. A., and Murphy, K., “The truth is hard to make: Validation of medical image registration,” in [*2016 23rd International Conference on Pattern Recognition (ICPR)*], 2294–2300, IEEE (2016).
- [10] Weitkamp, T., Scheel, M., Giorgetta, J., Joyet, V., Roux, V. L., Cauchon, G., Moreno, T., Polack, F., Thompson, A., and Samama, J., “The tomography beamline ANATOMIX at Synchrotron SOLEIL,” *Journal of Physics: Conference Series* **849**, 012037 (2017).
- [11] Desjardins, D., Carcy, A., Giorgetta, J., Meneglier, C., Scheel, M., and Weitkamp, T., “Design of Indirect X-Ray Detectors for Tomography on the Anatomix Beamline,” in [*Proc. 10th Mechanical Engineering Design of Synchrotron Radiation Equipment and Instrumentation (MEDSI’18), Paris, France, 25-29 June 2018*], *Mechanical Engineering Design of Synchrotron Radiation Equipment and Instrumentation*, 355–357, JACoW Publishing (Dec 2018).
- [12] Rodgers, G., Schulz, G., Deyhle, H., Kuo, W., Rau, C., Weitkamp, T., and Müller, B., “Optimizing contrast and spatial resolution in hard x-ray tomography of medically relevant tissues,” *Applied Physics Letters* **116**(2), 023702 (2020).
- [13] Thurner, P., Beckmann, F., and Müller, B., “An optimization procedure for spatial and density resolution in hard x-ray micro-computed tomography,” *Nuclear Instruments and Methods in Physics Research Section B* **225**(4), 599–603 (2004).
- [14] Klein, S., Staring, M., Murphy, K., Viergever, M. A., and Pluim, J. P. W., “elastix: A toolbox for intensity-based medical image registration,” *IEEE Transactions on Medical Imaging* **29**(1), 196–205 (2010).
- [15] Shamonin, D., Bron, E., Lelieveldt, B., Smits, M., Klein, S., and Staring, M., “Fast parallel image registration on CPU and GPU for diagnostic classification of Alzheimer’s disease,” *Frontiers in Neuroinformatics* **7**, 50 (2014).
- [16] Yushkevich, P. A., Piven, J., Hazlett, H. C., Smith, R. G., Ho, S., Gee, J. C., and Gerig, G., “User-guided 3d active contour segmentation of anatomical structures: Significantly improved efficiency and reliability,” *NeuroImage* **31**(3), 1116–1128 (2006).
- [17] Klein, S., Pluim, J. P. W., Staring, M., and Viergever, M. A., “Adaptive stochastic gradient descent optimisation for image registration,” *International Journal of Computer Vision* **81**(3), 227 (2008).
- [18] Lester, H. and Arridge, S. R., “A survey of hierarchical non-linear medical image registration,” *Pattern Recognition* **32**(1), 129–149 (1999).
- [19] Rueckert, D., Sonoda, L. I., Hayes, C., Hill, D. L. G., Leach, M. O., and Hawkes, D. J., “Nonrigid registration using free-form deformations: application to breast MR images,” *IEEE Transactions on Medical Imaging* **18**(8), 712–721 (1999).

- [20] Hansen, P. C., “The L-curve and its use in the numerical treatment of inverse problems,” in [*Computational Inverse Problems in Electrocardiology*, ed. P. Johnston, *Advances in Computational Bioengineering*], 119–142, WIT Press (2000).